

RSC Advances



This is an *Accepted Manuscript*, which has been through the Royal Society of Chemistry peer review process and has been accepted for publication.

Accepted Manuscripts are published online shortly after acceptance, before technical editing, formatting and proof reading. Using this free service, authors can make their results available to the community, in citable form, before we publish the edited article. This *Accepted Manuscript* will be replaced by the edited, formatted and paginated article as soon as this is available.

You can find more information about *Accepted Manuscripts* in the [Information for Authors](#).

Please note that technical editing may introduce minor changes to the text and/or graphics, which may alter content. The journal's standard [Terms & Conditions](#) and the [Ethical guidelines](#) still apply. In no event shall the Royal Society of Chemistry be held responsible for any errors or omissions in this *Accepted Manuscript* or any consequences arising from the use of any information it contains.

**Synthesis, characterization, and photocurrent generation of a new
nanocomposite based Cu-TCPP MOF and ZnO nanorod**

**Rahmatollah Rahimi^{*}, Samaneh Shariatinia, Solmaz Zargari, Marzieh Yaghobi Berijani,
Ali Ghaffarinejad, **Zahra Sadat Shojaie****

¹Department of Chemistry, Iran University of Science and Technology, Tehran 16846-13114, Iran

*Corresponding author

E-mail address: rahimi_rah@iust.ac.ir

Tel: 02177240290, Fax: +98-021-77491204

Abstract

A series of MOF–ZnO nanocomposites with different content of ZnO nanorods were synthesized via a facile hydrothermal reaction. X-ray diffraction (XRD), UV-vis spectroscopy, field-emission scanning electron microscopy (FE-SEM), EDX, BET and FT-IR were employed to characterize the prepared samples. According to the UV-Vis spectroscopy, the porphyrin center was filled with a Cu atom in Cu–TCPP. BET analysis shows that the surface area of Cu-TCPP MOF-ZnO nanorods composite was decreased compared to Cu-TCPP MOF. Therefore, ZnO nanorods covered on the surface of the Cu-TCPP MOF crystals and distributed between the MOF nanosheets. Photocurrent measurements determined that MOF–ZnO nanocomposite with 15% of ZnO nanorod exhibited higher photoactivity under visible light irradiation. In the prepared nanocomposite, MOF sheets act as electron transport channels to efficiently separate the photogenerated charge carriers from ZnO nanorods. It is hoped that our current work could promote increased interest in designing the nanocomposites of one-dimensional semiconductor and two-dimensional MOFs for different photoassisted applications.

Keywords: Porphyrin, Metal organic framework, ZnO nanorod, Photocurrent generation

Introduction:

Photocurrent measurement could feasibly be an analytical tool of low cost and high sensitivity due to the plentiful availability of substrates, repeatable use and elimination of undesired background signals by light excitation and current detection [1, 2]. This process is based on the electron transfer among an electrolyte, a semiconductor, and an electrode under the light illumination [3]. Photoelectrochemical method is more sensitive than electrochemical method

[4]. Electrochemical method has some unwanted background signals. In photoelectrochemical method, the excitation source (light) and the detection signal (photocurrent) are separated. Therefore, both optical and electrochemical methods together, eliminate these background signals [5]. Nowadays, researchers in this field continue to be devoted to new materials and assembly of photosensitizers for more an efficient conversion of light into electricity and rapid photoresponse [6, 7]. Ahmed and coworkers prepared a film on ITO of porphyrin-polyoxometalate hybrid material by the Langmuir-Schaefer inverted transfer method. Photocurrent generation was measured to determine the photovoltaic performance of the prepared Langmuir-Schaefer film. The results determined that porphyrin as an electron donor and light harvesting agent, significantly increases the photocurrent response of prepared film [8]. Porphyrin dyes and their derivatives play an important function in several applications, such as solar energy conversion [9], medical imaging [10], photo therapy [11], photocatalysis [12] and sensing [13]. Due to their broad light absorption and preferable photoelectric activity, photoelectrochemical cell based porphyrin photosensitizer can be used as a simple model of charge separation and electron transport which occur in nature [14]. Furthermore, they act as an agent in energy conversion devices such as dye sensitized solar cells [15]. In 2014, Zahao and coworkers prepared porphyrin-[60] fullerene polymers to generate photocurrent. In the synthesized polymer, the efficient photoinduced electron transfer from singlet excited porphyrin to fullerene. The linking of porphyrin to fullerene resulted in the formation of charge separated state with a lifetime as long as 140 μs [16]. Investigation to devote an efficient photosensitizer for high conversion of light into electricity and rapid photoresponse is currently under intensive research and development.

Metal-organic frameworks (MOFs), or porous coordination polymers (PCPs), are a class of crystalline hybrid materials with unique optical and electrical properties [17]. These compounds form by the connection of metal centers or clusters, as nodes and coordinating ligands as linkers, which impart high porosity in the MOFs structure [18, 19]. Some of the unique properties of MOFs are the large surface area, ordered crystalline structure, and highly regularized pores [20]. During the past decade MOFs have potential for useful applications including fuel cells, solar cells, and catalysis processes [21]. Organic ligands play an important role in the application of MOFs. In porphyrin based MOFs, porphyrin chromophores are assembled into ordered supramolecular solids which yields high-performance photoactive materials.

Tetrakis(4-carboxyphenyl)porphyrin (TCPP) is a prototypical chromophore which has been used as a building block in MOFs and photovoltaic applications [22, 23]. In the TCPP based MOFs the formed C-O-metal bond between TCPP and metal node could act as the electron transfer channel, facilitating the electron injection from excited porphyrin units to metal nodes in the MOF structure [24, 25, 26]. On the other world, carboxylate ligand accelerates the ligand-to-metal (LMCT) charge transfer and site-to-site electron migration within the MOF structure.

Silien and coworkers grew a series of metal organic coordination films with TCPP and trimesic acide ligands and Cu^{2+} ion linkers on ITO electrodes. The generated photocurrent determined that TCPP was photoexcited in this blend and photogenerated charges were transported across the metal-organic multilayers [27].

The principle objective of the present research is to prepare an efficient visible-light photoelectrode to significantly use the visible light in the photocurrent generation process. Recently, MOF composites have been promoted increasing interest due to their various applications [28]. These composites show novel functionalities compared to their individual

components alone [29, 30]. Yan and coworkers assembled a photoactive molecule into MOFs system as a host-guest material toward potential photofunctional applications. It was suggested that the encapsulated molecule can further modify the electronic structure of the host MOF materials [31].

Herein, we composited Cu-TCPP MOF with ZnO nanorods. ZnO is a II-VI semiconductor with a wide band gap and high transmittance in the visible region [32]. The selection of suitable metal oxide semiconductors is a crucial step to achieve high photoactivity. ZnO as a large-band-gap semiconductor and photoactive material has been attracted to great attention in recent years due to the excellent electrical and optical properties [33]. This material has been used in many fields such as light-emitting diodes, ultraviolet lasers, chemical sensors, solar cells, and so on [34]. ZnO has been widely used as a photoanode in dye-sensitized solar cells [35]. ZnO is a n-type semiconductor [36] and the d orbital of Zn^{2+} in ZnO is full of electron. Therefore, upon the irradiation of light, the photoexcited electrons to be easily transferred out of ZnO to generate a high current [37].

In our experiment, a new nanocomposite was prepared based porphyrin MOF and ZnO nanorods. Despite the fact that porphyrins were developed and used in solar cells [15], no report on the photocurrent generation from nanocomposite based porphyrin MOF and ZnO nanorods appeared in the literature up to now. In this MOF, we use TCPP as a linker and Cu as a node. Due to the acceleration of the carboxyl group of TCPP in LMCT, high conductivity of Cu atom [38], and high capability of ZnO in photocurrent generation, the prepared Cu-TCPP MOF/ZnO nanocomposite is expected to play an important role in the increasing of photocurrent. Furthermore, the porphyrin MOF and ZnO nanorod effect on photocurrent generation was investigated and discussed in details.

Experimental section

Synthesis of ZnO nanorods

ZnO nanorods were prepared according to a method described earlier [39]. ZnO nanorods were grown in 50 mL of equimolar (0.1 M) aqueous solution of zinc nitrate, $\text{Zn}(\text{NO}_3)_2 \cdot x\text{H}_2\text{O}$, and hexamethylenetetramine (HMTA; $\text{C}_6\text{H}_{12}\text{N}_4$) in a conventional reaction flask with a reflux condenser. The reaction temperature was 95 °C. The reaction time was 8 h for growth of nanorods.

Synthesis of MOF-ZnO nanocomposite

Tetrakis(4-carboxyphenyl)porphyrin (TCPP) was prepared according to our previous report [24]. Cu-TCPP MOF was synthesized by the solvothermal reaction of $\text{Cu}(\text{NO}_3)_2 \cdot 3\text{H}_2\text{O}$ and TCPP in a mixture of N,N-dimethylformamide and ethanol [40]. To prepare Cu-TCPP MOF/ZnO nanocomposite, TCPP (0.03 mmol), $\text{Cu}(\text{NO}_3)_2 \cdot 3\text{H}_2\text{O}$ (0.03 mmol), DMF 4.5 mL, and ethanol 1.5 mL were mixed at room temperature. After that, a calculated concentration of the prepared ZnO nanorod solution was added to the mixture. Then the mixture was heated to 80 °C in 30 minutes, kept at 80 °C for one day and then slowly cooled to 25 °C at 5 °C/h. The synthesized purple powder was washed with ethanol and collected by centrifuging. Cu-TCPP MOF/ZnO nanocomposites with three different content of ZnO nanorods (10, 15, and 20 wt%; actual content was indicated by ICP analysis) were prepared.

Photoelectrochemical measurements

Photocurrent response measurements were carried out using a homemade three-electrode cell using a KCl-saturated Ag/AgCl electrode, a platinum rod, and Fluorine doped tin oxide (FTO)

glass coated with the prepared photoactive materials as the reference, counter, and working electrodes, respectively. A 20 W white LED lamp was used as a visible light source. The working electrode was prepared by a drop cast method. Briefly, 15 mg of the prepared photoactive material was suspended in 0.15 ml EtOH to make a slurry solution. Then, identical volume of the slurry was dropwised using a micropipette on the surface of FTO glass to cover the whole surface of the electrodes. The prepared electrodes were dried at 60 °C. An attempt was made to prepare the electrodes in a way that the thickness and morphology of the prepared compounds became homogeneous on the surface of FTO. The actual dimensions of the prepared electrodes was 1.5 in 2 cm.

Analytical methods

Fourier transform infrared spectra were recorded by a FTIR-8400S spectrophotometer (Shimadzu, Japan) in the range of 400-4000 cm^{-1} . The X-ray powder diffraction was recorded by an XRD diffractometer (Philips X'pert, Netherlands) equipped with Cu $k\alpha$ radiation ($\lambda = 1.5406$ °A) in a 2θ range of $5^\circ \leq 2\theta \leq 80^\circ$. The surface areas of the materials were determined using the Brunauer–Emmett–Teller (BET) method from N_2 adsorption and desorption isotherms which were measured on a Micromeritics ASAP2020 system. The pore size distribution was calculated from desorption branches of the nitrogen isotherms applying the Barrett–Joyner–Halenda (BJH) methods. The structural morphology of the samples was observed by a scanning electron microscope (SEM, LEO 1455VP (Cambridge, U.K)) and transmission electron microscopy (TEM) was carried out using an EM10C-100 kV series microscope that was purchased from the Zeiss Company, Germany. The UV-vis spectra were performed using a

double-beam UV spectrophotometer (Shimadzu UV-1700). Photocurrent response measurements were performed with a potentiostat/galvanostat (μ Autolab, Type II).

Characterization of the prepared samples

XRD Analysis

The XRD patterns of the ZnO nanorods, Cu-TCPP MOF, and Cu-TCPP MOF/ZnO nanocomposites are shown in Fig. 1. All the diffraction peaks in the ZnO XRD pattern are indexed as the hexagonal wurtzite ZnO structure. According to JCPDS card number 36-1451, the peaks at 2θ values of 31.8, 34.4, 36.3, 47.5, 56.6, 62.9, 66.4, 68.0, 69.1, 72.6 and 77.0 can be indexed to (100), (002), (101), (102), (110), (103), (200), (112), (201), (004), and (202) crystal planes, respectively. No other impurity peaks were detected [41].

The XRD patterns of prepared Cu-TCPP MOF is identical to that reported in the literature, verified the correction of MOF synthesis [40]. **The highly ordered in-plane molecular arrangement in Cu-TCPP MOF consists of a "checkerboard" motif of Cu-centered TCPP units linked by binuclear $\text{Cu}_2(\text{COO})_4$ paddle wheels [42]. In the XRD patterns of the prepared MOF all of the reflections could be indexed as (hkl) of the pseudo-2D tetragonal unit cell [40].**

<Fig. 1>

As shown in the XRD patterns of the as-prepared nanocomposites, the XRD patterns are the same for Cu-TCPP MOF/ZnO nanocomposites with different weight addition ratios of ZnO. **It is seen that the Cu-TCPP MOF nanocomposite with 10, 15, 20% contents of ZnO nanorods show similar XRD patterns as same as Cu-TCPP MOF and no characteristic peaks of ZnO nanorods are**

observed in these XRD patterns. This is probably because of the relatively low content of ZnO nanorods in the prepared nanocomposites or over shadow of MOF on ZnO nanorod. However, with the addition ratio of ZnO nanorods at 80%, the main characteristic peaks belonging to the separate ZnO nanorods can be identified in the XRD pattern. The characteristic peaks of Cu-TCPP MOF and ZnO nanorods are seen in the XRD patterns of this prepared nanocomposite. Therefore, both MOF and ZnO nanorods are present in the prepared nanocomposite.

UV-Vis spectroscopy of Cu-TCPP MOF and prepared nanocomposites

UV-Vis spectroscopy is an efficient and powerful method to determine the metalation of porphyrin. Porphyrins consist the characteristic peaks of one solet band in about 400 nm and four Q bands in the range of 500-700 nm. The number of Q bands decreased from four in porphyrin to two in metalloporphyrin, which demonstrates that the porphyrin center in metalloporphyrin has been filled with metal atom [43, 44]. This is because with metalation the symmetry of molecules is increased from C_{2v} for porphyrin to D_{4h} for metalloporphyrin [2, 3].

The UV-Vis spectra of TCPP, Cu-TCPP MOF, and prepared nanocomposites was studied in basic solution (1M NaOH) that was used for dissolving the prepared materials. MOF was shown to contain only one porphyrin species. The number of Q bands decreased from four in H_2 TCPP to one in Cu-TCPP MOF, which demonstrates that the porphyrin center in Cu-TCPP MOF has been filled with a Cu atom [43]. As shown in curves b-d of Fig. 2, it is determined that the UV-Vis spectroscopy of Cu-TCPP MOF was unchanged in the presence of ZnO nanorods during the preparation of the nanocomposites.

<Fig. 2>

FT-IR Spectroscopy

The FT-IR spectra of TCPP and Cu–TCPP MOF are compared in Fig. 3. As shown in Fig. 3 (Curve f), a strong C=O stretching band can be observed at approximately 1700 cm^{-1} in the FT-IR spectrum of pure TCPP [24]. Cu–TCPP MOF and prepared nanocomposites shows an almost vanished peak around 1700 cm^{-1} and two new peaks at 1620 and 1400 cm^{-1} , which indicates the coordination of the carboxyl group in TCPP to the Cu atom.

<Fig. 3>

Morphological Characterization

Scanning electron microscopy (SEM) images were taken to directly analyze the morphology of the prepared samples and the effect of compositing on the microscopic structure of the samples, are displayed in Fig. 4. As can be seen in the Fig. 4A, 3D flower-like Cu–TCPP MOF was prepared through a solvothermal process. The thickness of each sheet in the prepared Cu–TCPP MOF was 15–20 nm. Furthermore, no other morphologies can be detected, indicating a high uniformity of the product with the 3D hierarchical flower-like morphology. It can be observed from Fig. 4B that the diameter of blank ZnO nanorods were 100–300 nm. The results demonstrate that the one-dimensional ZnO nanorods were deposited onto Cu–TCPP nanosheets with a unique two-dimensional structure during the hydrothermal process. With regard to the SEM images of Cu–TCPP/ZnO nanocomposite (Fig. 4C) in the presence of ZnO nanorods, the morphology of MOF nanosheets was changed. On the other hand, ZnO nanorods are not seen in the SEM images of nanocomposites. Therefore, they were wrapped by Cu–TCPP nanosheets.

The EDX analysis of Cu-TCPP/ZnO nanocomposite is shown in Fig. 4D, verified the presence of both Cu and Zn atom in the Cu-TCPP/ZnO nanocomposite structure.

<Fig. 4>

The morphology of the Cu-TCPP MOF/ZnO nanocomposite was further investigated by transmission electron microscopy (TEM). In the TEM images of the prepared nanocomposite, ZnO nanorods are seen on the surface of MOF nanosheets. Therefore, ZnO nanorods encapsulated into the Cu-TCPP MOF during the preparation process.

<Fig. 5>

BET Analysis

The specific surface area and porosity of the as-prepared Cu-TCPP MOF and Cu-TCPP MOF/ZnO nanocomposite were investigated using nitrogen adsorption and desorption isotherms (Fig. 6A). As shown in this figure, CuTCPP-MOF and Cu-TCPP MOF/ZnO nanocomposite display a type IV with H2 hysteresis loop N₂ adsorption isotherms which is attributed to mesoporous solids according to the IUPAC classification. The obvious decrease of the surface area and pore size distribution (fig. 6B) from Cu-TCPP MOF/ZnO nanocomposite to the Cu-TCPP MOF illustrates that ZnO nanorods covered the surface of the Cu-TCPP MOF crystals and distributed between the MOF nanosheets.

<Fig. 6>

Light-induced photocurrent investigation

A schematic illustration of the photoelectrochemical system fabricated using the Cu-TCPP MOF/ZnO nanocomposite modified electrode is shown in scheme 1. To investigate the influence of ZnO nanorod and Cu-TCPP MOF compositing on the photoelectrochemical properties of the prepared nanocomposite, the photocurrent response was measured under visible light irradiation. To investigate the power of light on the photocurrent response the 5 and 20 W white LED lamp was investigated in the photocurrent generation process. As shown in Fig. 7, the generated photocurrent with 20 W LED lamp was higher than 5 W LED lamp. Therefore, the 20 W LED lamp was used in the photocurrent generation process. The photocurrent intensity is related to the wavelength of the light [45]. The spectra of the 20 W white LED lamp is shown in the inset of Fig. 7. The diffuse reflectance spectrum of the prepared nanocomposite is shown in Fig. 7. As shown in this figure the prepared MOF nanocomposite can absorb the irradiation in the visible light range. In addition, the white LED lamp has a peak at 460 nm and a broad peak in the range of 500-650 nm. Therefore, a complete correspondence is observed between absorption ability of prepared MOF composite and the used white LED lamp.

<Fig. 7>

The results of photocurrent generation using ZnO, Cu-TCPP MOF, Cu-TCPP MOF/ZnO (10%), Cu-TCPP MOF/ZnO (15%), and Cu-TCPP MOF/ZnO (20%) electrodes are shown in Fig. 8B. The sample was irradiated under visible light for 20 s and kept in the dark for another 20 s. It is notable that the responses of the photocurrent were reproducible during the repeated on-off cycles under visible light irradiation. Therefore, the reproducible photocurrent responses without

a noticeable decrease in their relative intensities demonstrates the mechanical and photophysical stabilities of the electrode. A sharp photocurrent was generated when the Cu-TCPP MOF/ZnO (15%) electrode was subjected under irradiation of visible light. Photo-enhanced current at applied potential 0.1 V vs. SCE reference electrode is found about $1.8 \mu\text{A}/\text{cm}^2$. Compared with the Cu-TCPP MOF electrode, Cu-TCPP MOF/ZnO (15%) electrode exhibited a 6.5 fold enhancement of photocurrent intensity.

<Fig. 8>

Mechanism

Electrically conducting porous MOFs have attracted considerable interest over the past several decades. Charge mobility in MOFs achieve by coupling between π orbitals of ligand and d orbitals of metal [17]. In Cu-TCPP MOFs, π stacking electroactive porphyrin molecules are capable in charge transporting in the MOFs structure [46]. In Cu-TCPP MOF, Cu atom is coordinated by four carboxylate oxygen atoms. Therefore, the oxygen atoms interact with the d orbital of Cu and promoting charge delocalization along the (-Cu-O-) chain. This process named as a 'through bond' strategy for achieving charge delocalization [47].

Furthermore, MOF-based light-harvesting devices present many opportunities for power generation [48]. Compared to porphyrin light-harvesting system [24, 49], MOFs possess long-range order that eliminates local variations known to reduce efficiency in disordered metal oxides sensitized with porphyrins. In Cu-TCPP MOF, porphyrin units are capable of capturing photon because of their strong absorption bands [50].

As shown in Fig. 7B the highest photocurrent was generated by Cu-TCPP MOF/ZnO (15%) nanocomposite. Composition of Cu-TCPP MOF with ZnO nanorods is an efficient approach to improving light harvesting and electron transferring within the MOF structure. As mentioned

earlier ZnO is the large-band-gap and n-type semiconductor. Furthermore, upon the irradiation of light, the photoexcited electrons to be easily transferred from ZnO to generate a high current [51]. Nevertheless, high recombination rate of photogenerated electron-hole pairs limits the utilization of pure ZnO nanorods as a photoactive material [52].

<Scheme 1>

The mechanism of photoexcitation and charge transfer in Cu-TCPP MOF/ZnO nanocomposite is summarized in scheme 1 (the chemical potentials were calculated by cyclic voltammetry measurement). In Cu-TCPP MOF/ZnO nanocomposite, upon irradiation of light, the TCPP molecule is excited into the singlet state. The ligand-to-metal charge transfer (LMCT) occurs in the MOF structures [53]. The photogenerated electron from CuTCPP transfer to the Cu atom through bond strategy, which cause to decrease the recombination of electron-hole in porphyrin units. This electron migrates site-to-site within Cu-TCPP MOF structure. The photocurrent is generated by the reduction of O₂ [54] at the interface and by transfer of electrons from the reduced O₂ (O₂⁻) to the porphyrin cation units in MOF structure. Therefore, the ground-state of porphyrins is recovered.

Furthermore, the photogenerated electron is transferred to the conduction band of ZnO nanorod. This electron can be transferred to the FTO electrode and then photocurrent is generated. In this nanocomposite, MOF sheets act as electron transport channels to efficiently separate the photogenerated charge carriers from ZnO nanorods. The improved photoactivity of Cu-TCPP/ZnO nanocomposite can be ascribed to the synergistic effect of enhanced light absorption capacity, decrease in recombination of photogenerated electron-hole pairs and effective interfacial composition between Cu-TCPP MOF and ZnO nanorods. The photocurrent responses of Cu-TCPP MOF/ZnO nanocomposites showed that the photocurrent was decreased beyond an

optimum ZnO nanorods concentration (15%). This is because the photoactive sites of Cu-TCPP MOF were shielded with ZnO nanorods through an increase in the ZnO nanorods content.

Conclusion

For the first time, Cu-TCPP MOF/ZnO nanocomposite was prepared via the hydrothermal method. UV-Vis spectroscopy determined that the porphyrin center in Cu-TCPP was filled with Cu atom. According to the BET analysis, surface area of Cu-TCPP MOF/ZnO nanocomposite was decreased compared to Cu-TCPP MOF. Therefore, ZnO nanorods covered on the surface of the Cu-TCPP MOF crystals and distributed between the MOF nanosheets.

Cu-TCPP MOF/ZnO (15%) electrode exhibited a 6.5 fold enhancement of photocurrent intensity compared to the Cu-TCPP MOF electrode. The high photoactivity of Cu-TCPP MOF/ZnO (15%) nanocomposite is due to the unique porous structure, excellent light harvesting properties, facilitated site-to-site energy migration within the Cu-TCPP MOF structure, easy electron injection through the Cu-TCPP MOF to the conduction band of ZnO, and low recombination in ZnO nanorods and porphyrin units.

Acknowledgments

The authors gratefully acknowledge the financial support of the Chemistry Department, Iran University of Science and Technology, provided in the form of a Faculty Internal Research Grant awarded to the corresponding author, which provided the necessary funding for this research. The authors would also like to thank the anonymous reviewers for their detailed and insightful comments on an earlier draft of this article.

References

- [1] M. Elborg, T. Noda, T. Mano, M. Jo, Y. Sakuma, K. Sakoda, L. Han, *Sol. Energy Mater. Sol. Cells*, 2015, **134**, 108-113.
- [2] H. Geng, C. M. Hill, Sh. Zhu, H. Liu, L. Huang and Sh. Pan, *RSC Adv.*, 2013, **3**, 2306-2312
- [3] M. Freitag, E. Galoppini, *Energy Environ. Sci.*, 2011, **4**, 2482-2494.
- [4] A. Ikeda, M. Nakasu, Sh. Ogasawara, H. Nakanishi, M. Nakamura, J. I. Kikuchi, *Org. Lett.*, 2009, **11**, 1163-1166.
- [5] W. Lu, Y. Jin, G. Wang, D. Chen, J. Li, *Biosens. Bioelectron.*, 2008, **23**, 1534-1539.
- [6] R. T. P. Gopinath and H. John, *RSC Adv.*, 2014, **4**, 29901-29908
- [7] P. Wang, X. Wen, R. Amal and Y. H. Ng, *RSC Adv.*, 2015, **5**, 5231-5236
- [8] I. Ahmed, R. Farha, Z. Huoe, C. Allain, X. Wangg, H. Xu, M. Goldmann, B. Hasenknop, L. Ruhlmann, *Electrochim. Acta*, 2013, **110**, 726-734.
- [9] S. D. Pop, S. P. Kate, J. Rappich, K. Hinrichs, *Sol. Energy Mater. Sol. Cells*, 2014, **127**, 169-173.
- [10] F. Lv, L. Mao, T. Liu, *Mater. Sci. Eng. C*, 2014, **43**, 221-230.
- [11] M. R. Parida, S. M. Aly, E. Alarousu, O. F. Mohammed, *J. Phys. Chem. C*, 2015, **119**, 2614-2621.
- [12] Sh. Afzal, W. A. Daoud, S. J. Langford, *ACS Appl. Mater. Interfaces*, 2013, **5**, 4753-4759.
- [13] Y. Hu, Zh. Xue, H. He, R. Ai, X. Liu, X. Lu, *Biosens. Bioelectron.*, 2013, **47**, 45-49.

- [14] P. K. B. Palomaki, M. R. Civic, P. H. Dinolfo, *ACS Appl. Mater. Interfaces*, 2013, **5**, 7604–7612
- [15] K. Ladomenou, T. N. Kitsopoulos, G. D. Sharma and A. G. Coutsolelos, *RSC Adv.*, 2014, **4**, 21379-21404
- [16] H. Zhao, Y. Zhu, Ch. Chen, J. Zheng, *Polymer*, 2014, **55**, 1913-1916.
- [17] V. Stavila, A. A. Talin, M. D. Allendorf, *Chem. Soc. Rev.*, 2014, **43**, 5994-6010.
- [18] Y. Luan, Y. Qi, Zh. Jin, X. Peng, H. Gao and G. Wang, *RSC Adv.*, 2015, **5**, 19273-19278.
- [19] D. Yan, R. Gao, M. Wei, Sh. Li, J. Lu, D. G. Evans, X. Duan, *J. Mater. Chem. C*, 2013, **1**, 997-1004.
- [20] S. Abedi, A. Morsali, *ACS Catal.*, 2014, **4**, 1398–1403.
- [21] I. Ahmed, S. H. Jhung, *Mater. Today*, 2014, **17**, 136–146.
- [22] X. S. Wang, L. Meng, Q. Cheng, Ch. Kim, L. Wojtas, M. Chrzanowski, Y. Sh. Chen, X. P. Zhang, Sh. Ma, *J. Am. Chem. Soc.*, 2011, **133**, 16322–16325.
- [23] H. Tian, J. Oscarsson, E. Gabrielsson, S. K. Eriksson, R. Lindblad, B. Xu, Y. Hao, G. Boschloo, E. M. J. Johansson, J. M. Gardner, A. Hagfeldt, H. Rensmo, L. Sun, *Sci. Rep.* 2014, **4**, 4282.
- [24] R. Rahimi, M. Mahjoub Moghaddas, S. Zargari, *Sol-Gel Sci. Technol.*, 2013, **65**, 420-429.
- [25] R. Abe, K. Hara, K. Sayama, K. Domen, H. Arakawa, *J. Photochem. Photobiol., Chem.*, 2000, **137**, 63-69.
- [26] E. Bae, W. Choi, *J. Phys. Chem. B*, 2006, **110**, 14792–14799.
- [27] J. T. Joyce, F. R. Laffir, Ch. Silien, *J. Phys. Chem. C*, 2013, **117**, 12502–12509.

- [28] I. Ahmed, S. H. Jhung, *Mater. Today*, 2014, **17**, 136–146.
- [29] D. Yan, Y. Tang, H. Lin, D. Wang, *Sci. Rep.*, 2014, **4**, 4337.
- [30] Y. Tang, W. He, Y. Lu, J. Fielden, X. Xiang, D. Yan, *J. Phys. Chem. C*, 2014, **118**, 25365–25373.
- [31] D. Yan, G. O. Lloyd, A. Delori, W. Jones, X. Duan, *Chem. Plus. Chem.*, 2012, **77**, 1112–1118.
- [32] A. Mahroug, S. Boudjadar, S. Hamrit, L. Guerbous, *Mater. Lett.* 2014, **134**, 248-251.
- [33] Zh. Chen, N. Zhang, Y. J. Xu, *Cryst. Eng. Comm.*, 2013, **15**, 3022–3030.
- [34] Q. Li, V. Kumar, Y. Li, H. Zhang, T. J. Marks, R. P. H. Chang, *Chem. Mater.*, 2005, **17**, 1001-1006.
- [35] R. Jose, V. Thavasi, S. Ramakrishna, *J. Am. Ceram. Soc.*, 2009, **92**, 289–301.
- [36] D. C. Look, J. W. Hemsky, *Phys. Rev. Lett.*, 1999, **82**, 2552.
- [37] J. H. Liu, L. Saravanan, *Mater. Lett.*, 2014, **134**, 30-33.
- [38] Ch. Yan, D. Xue, *Cryst. Growth Des.*, 2008, **8**, 1849–1854.
- [39] A. Qurashi, M. Faiz, N. Tabet, M. W. Alam, *Superlattices Microstruct.*, 2011, **50**, 173–180.
- [40] G. Xu, T. Yamada, K. Otsubo, S. Sakaida, H. Kitagawa, *J. Am. Chem. Soc.*, 2012, **134**, 16524-16527.
- [41] Y. Guo, X. Cao, X. Lan, C. Zhao, X. Xue, Y. Song, *J. Phys. Chem. C*, 2008, **112**, 8832–8838.

- [42] S. Motoyama, R. Makiura, O. Sakata, H. Kitagawa, *J. Am. Chem. Soc.*, 2011, **133**, 5640–5643.
- [43] G. Xu, T. Yamada, K. Otsubo, Sh. Sakaida, H. Kitagawa, *J. Am. Chem. Soc.*, 2012, **134**, 16524–16527.
- [44] D. Marsh, L. Mink, *J. Chem. Educ.*, 1996, **73**, 1188.
- [45] J. B. Jiang, Y. Y. Wu, P. Wang, P. Huo, Q. Yu Zhu, J. Dai, *Dyes Pigments*, 2014, **107**, 153-160.
- [46] Sh. Wan, J. Guo, J. Kim, H. Ihee, D. Jiang, *Angew. Chem.*, 2009, **121**, 5547-5550.
- [47] Sh. Wan, J. Guo, J. Kim, H. Ihee, D. Jiang, *Angew. Chem.*, 2008, **47**, 8826-8830.
- [48] A. A. Talin, A. Centrone, A. C. Ford, M. E. Foster, V. Stavila, P. Haney, R. A. Kinney, V. Szalai, F. E. Gabaly, H. P. Yoon, F. Léonard, M. D. Allendorf, *Science*, 2014, **343**, 66-69.
- [49] R. Rahimi, E. H.Fard, S. Saadati, M. Rabbani, *J. Sol-Gel Science Technol.*, 2012, **62**, 351-357.
- [50] R. Rahimi, E. Gholamrezapor, M. R. Naimi-jamal, *Inorg. Chem. Commun.*, 2011, **14**, 1561-1568.
- [51] J. H. Liu, L. Saravanan, *Mater. Lett.*, 2014, **134**, 30-33.
- [52] Zh. Chen, N. Zhang, Y. J. Xu, *Cryst. Eng. Commun.*, 2013, **15**, 3022–3030.
- [53] D. Yan, R. Gao, M. Wei, Sh. Li, J. Lu, D. G. Evans, X. Duan, *J. Mater. Chem. C*, 2013, **1**, 997-1004.
- [54] J. T. Joyce, F. R. Laffir, Ch. Silien, *J. Phys. Chem. C*, 2013, **117**, 12502–12509.

Figure captions

Fig. 1. XRD patterns of the prepared samples: a) Cu-TCPP MOF, b) Cu-TCPP MOF/ZnO (10%), c) Cu-TCPP MOF/ZnO (15%), d) Cu-TCPP MOF/ZnO (20%), e) Cu-TCPP MOF/ZnO (80%) and f) ZnO nanorods

Fig. 2. UV-Vis spectra of a) Cu-TCPP MOF, b) Cu-TCPP MOF/ZnO (10%), c) Cu-TCPP MOF/ZnO (15%), d) Cu-TCPP MOF/ZnO (20%), and e) TCPP

Fig. 3. FT-IR spectra of the prepared samples: a) prepared ZnO nanorods, b) Cu-TCPP MOF/ZnO (20%), c) Cu-TCPP MOF/ZnO (15%), d) Cu-TCPP MOF/ZnO (10%), e) Cu-TCPP MOF, and f) TCPP

Fig. 4. SEM images of a) Cu-TCPP MOF, b) prepared ZnO nanorods, c) Cu-TCPP MOF/ZnO (15%), and d) EDX of Cu-TCPP MOF/ZnO (15%)

Fig. 5. TEM images of the Cu-TCPP MOF/ZnO (15%) nanocomposite.

Fig. 6. A) Nitrogen adsorption and desorption isotherms of a) Cu-TCPP MOF and b) Cu-TCPP MOF/ZnO (15%), B) Corresponding pore size distribution curve of a) Cu-TCPP MOF and b) Cu-TCPP MOF/ZnO (15%)

Fig. 7. Diffuse reflectance spectrum of the Cu-TCPP MOF/ZnO nanocomposite; Spectrum of the white LED lamp is shown in the inset.

Fig. 8. Photocurrent responses with on-off irradiation from A) 5W white LED, B) 20 W white LED in Na₂SO₄ aqueous solution (0.25 M); a) MOF, b) 20%, c) ZnO, d) 10%, and e) 15%; Applied potential +0.1 V vs SCE

Scheme 1. Schematic representation of the Cu-TCPP MOF/ZnO (15%) nanocomposite on an FTO substrate in the photoelectrochemical cell and the mechanism of the photocurrent generation

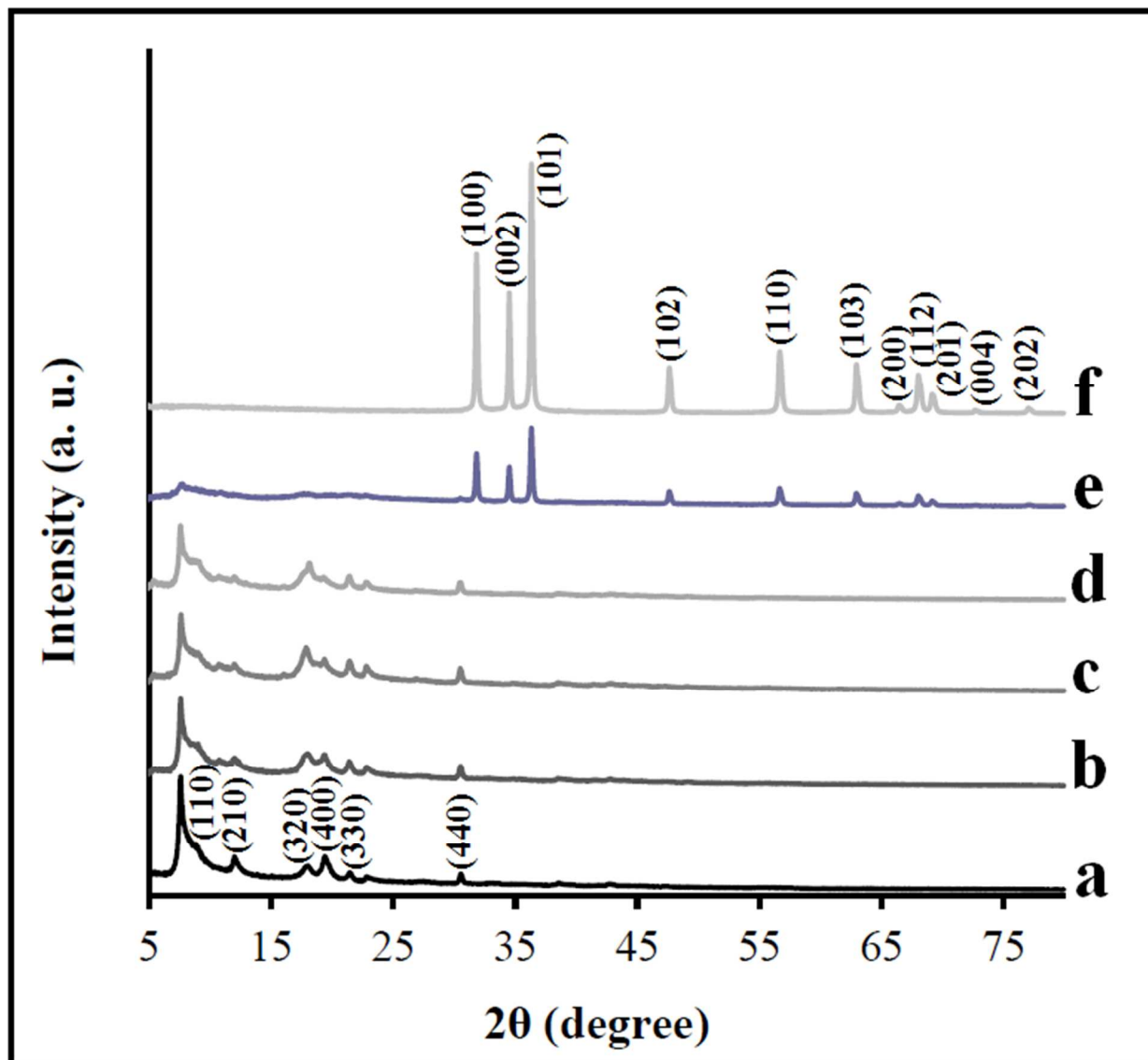


Fig. 1

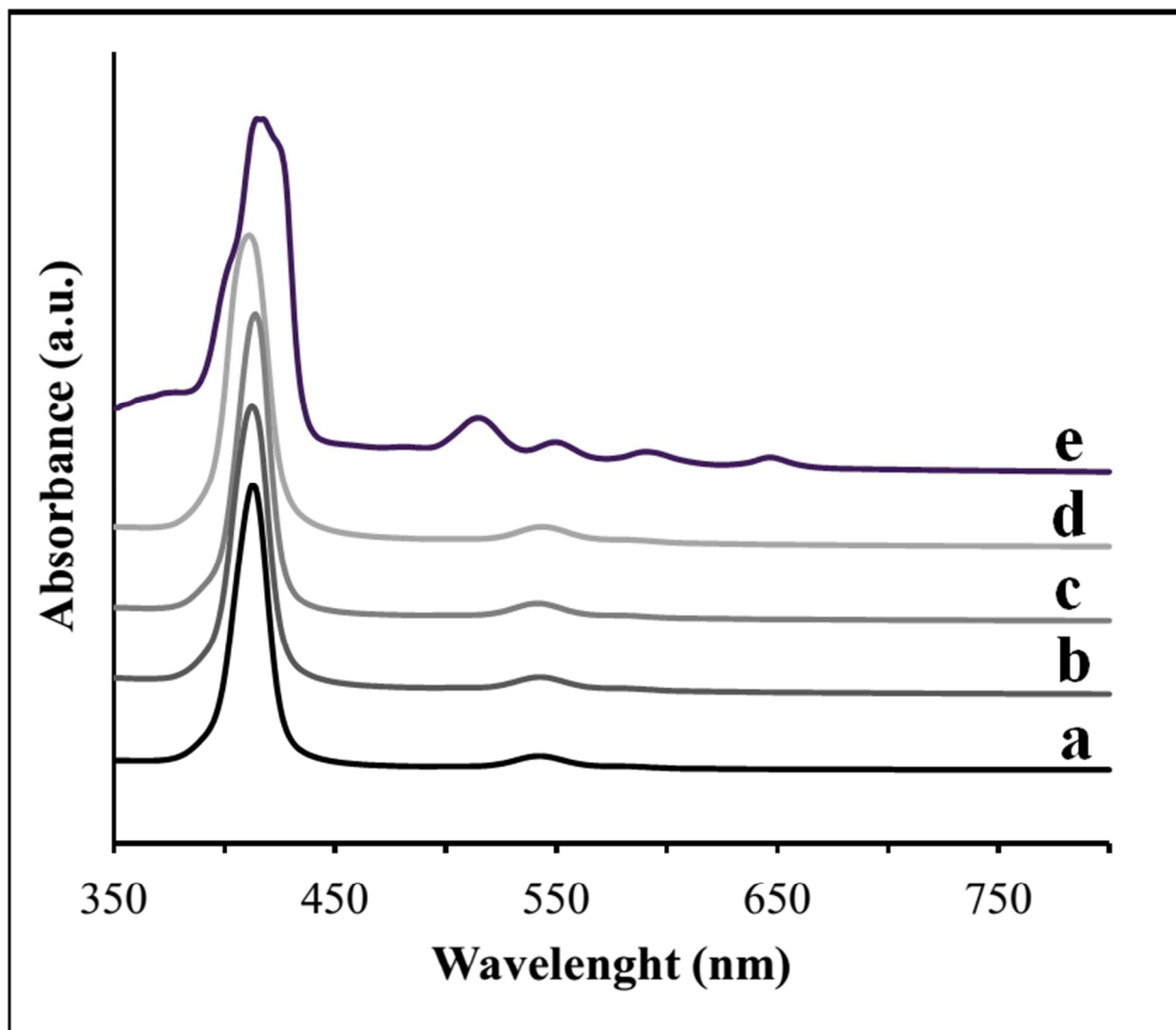


Fig. 2

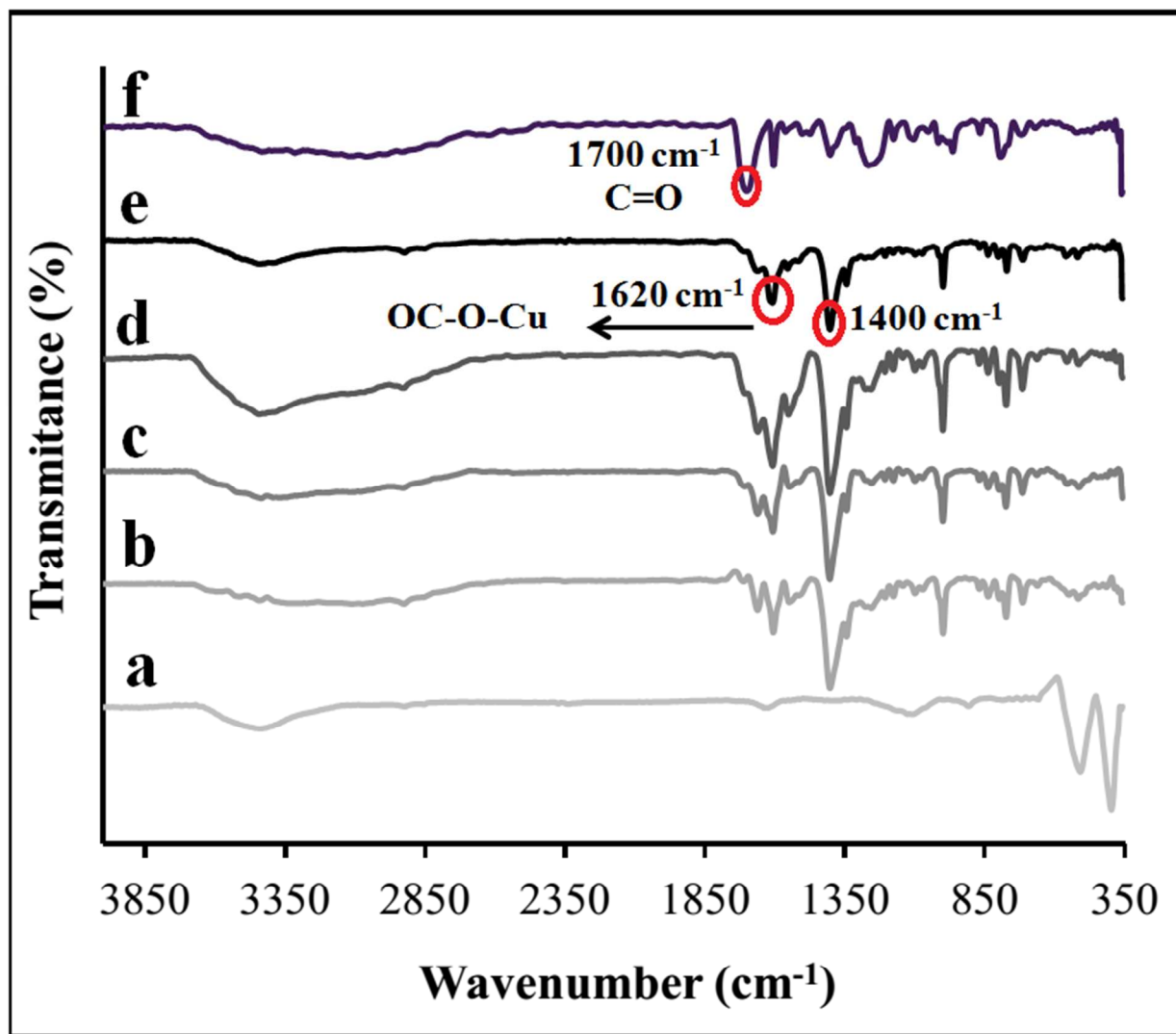


Fig. 3

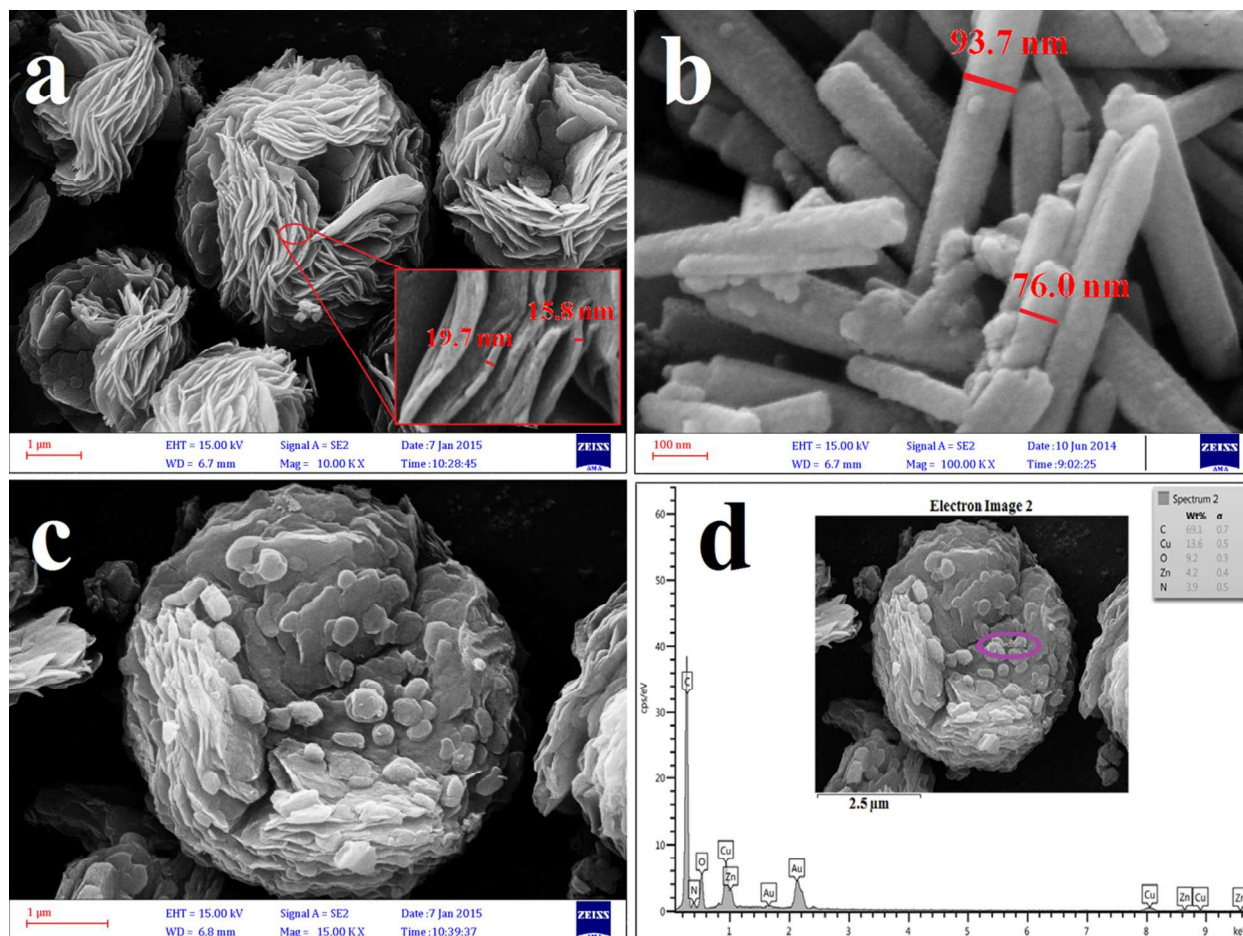


Fig. 4

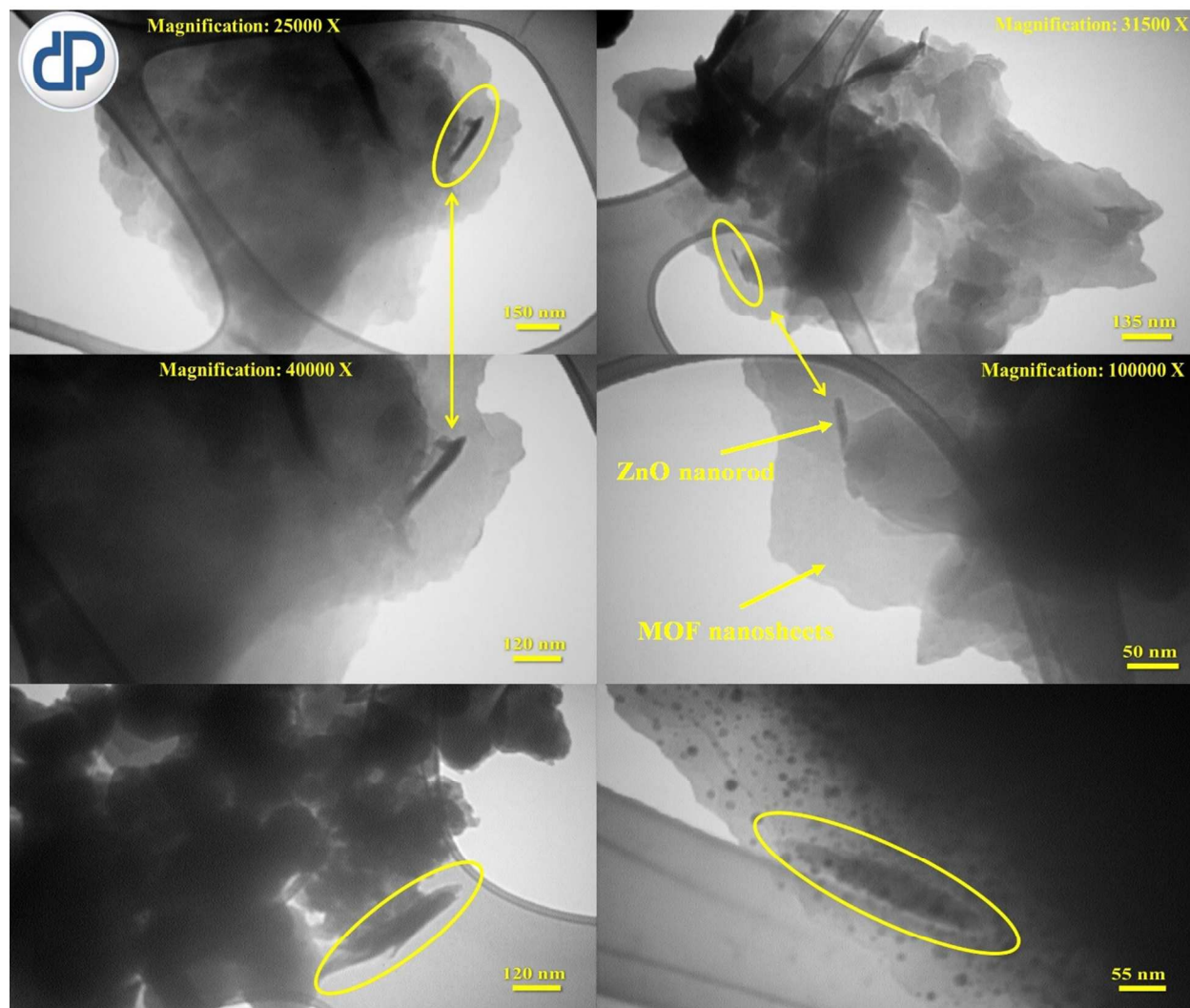


Fig. 5

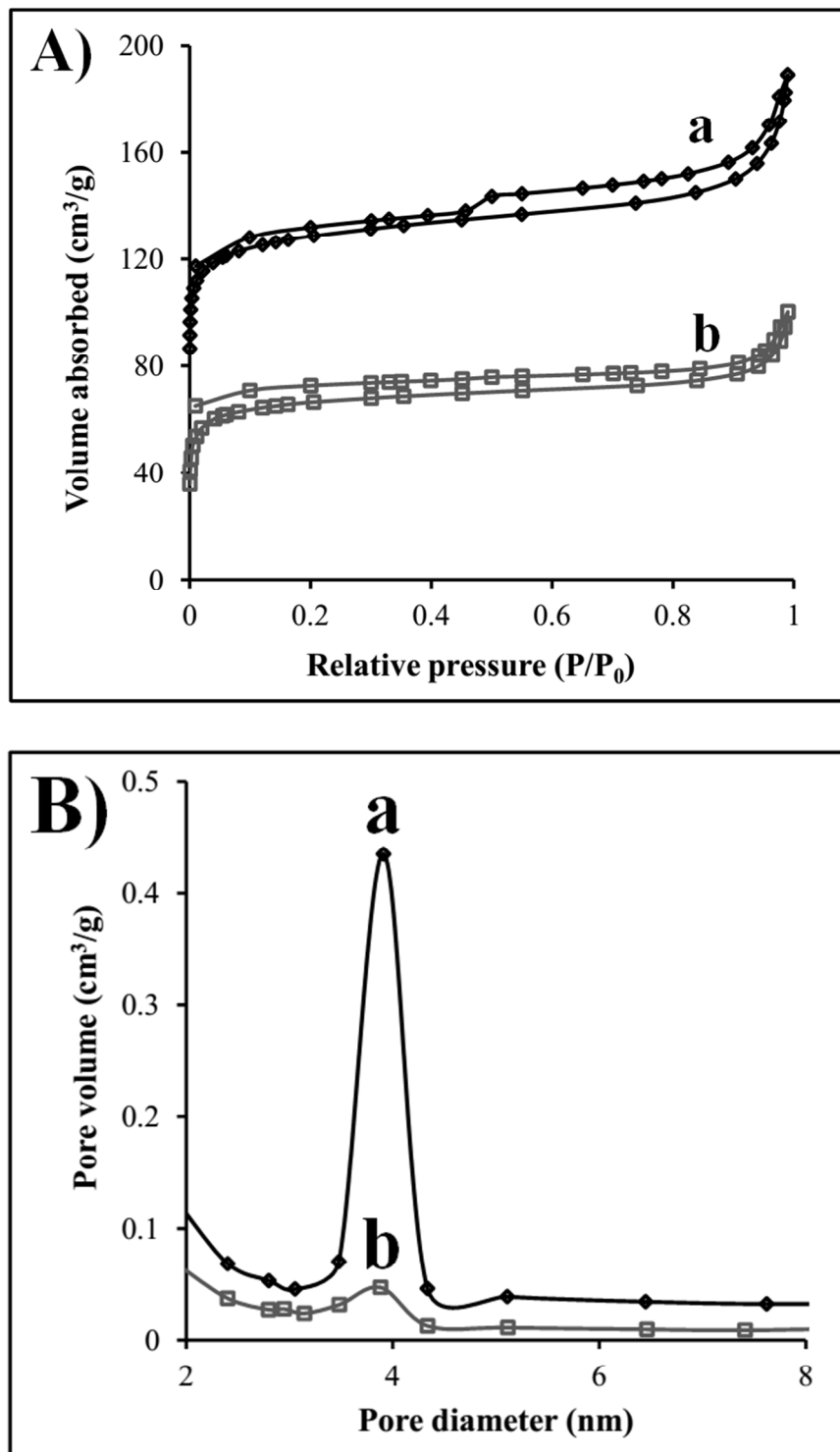


Fig. 6

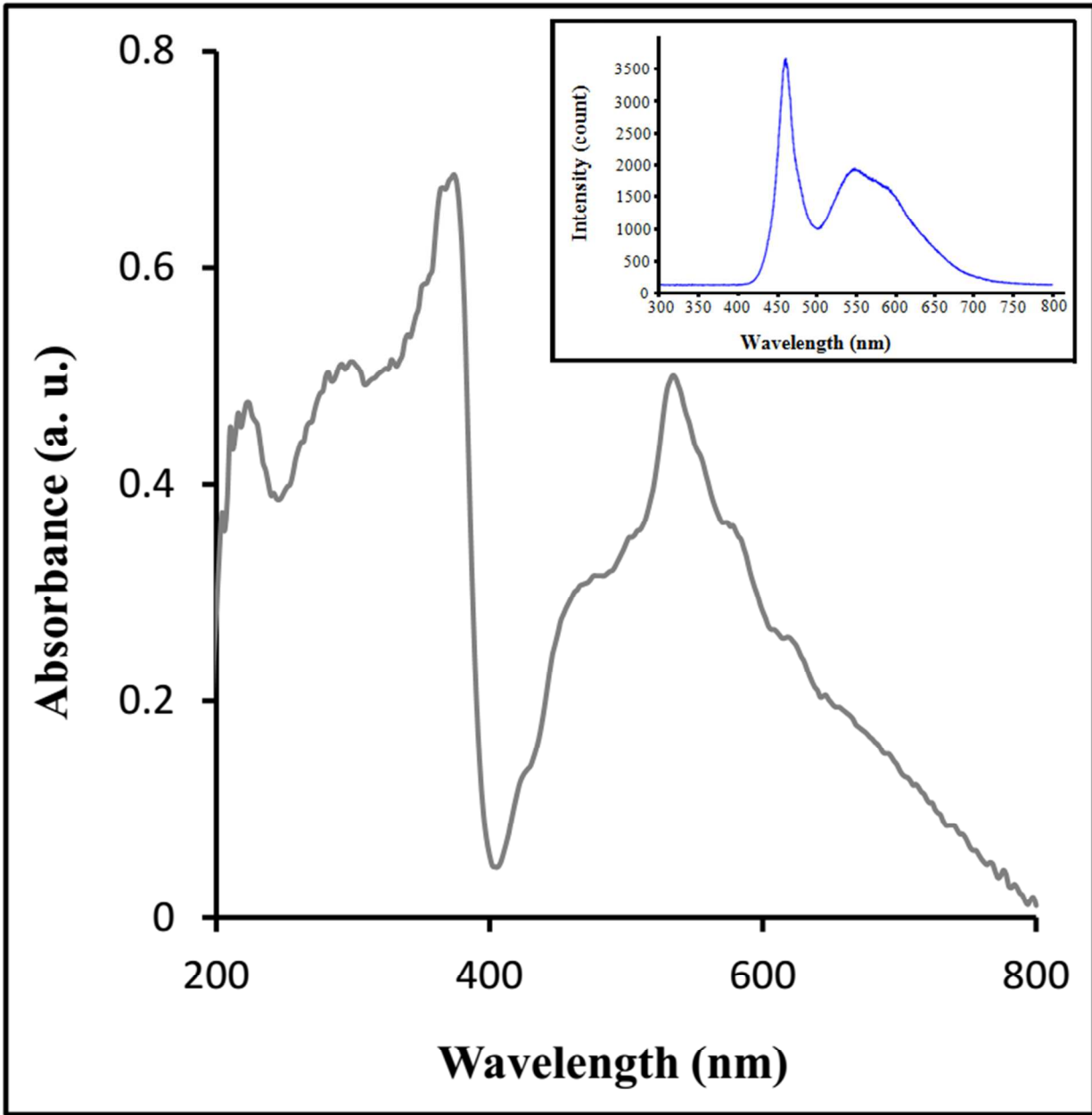


Fig. 7

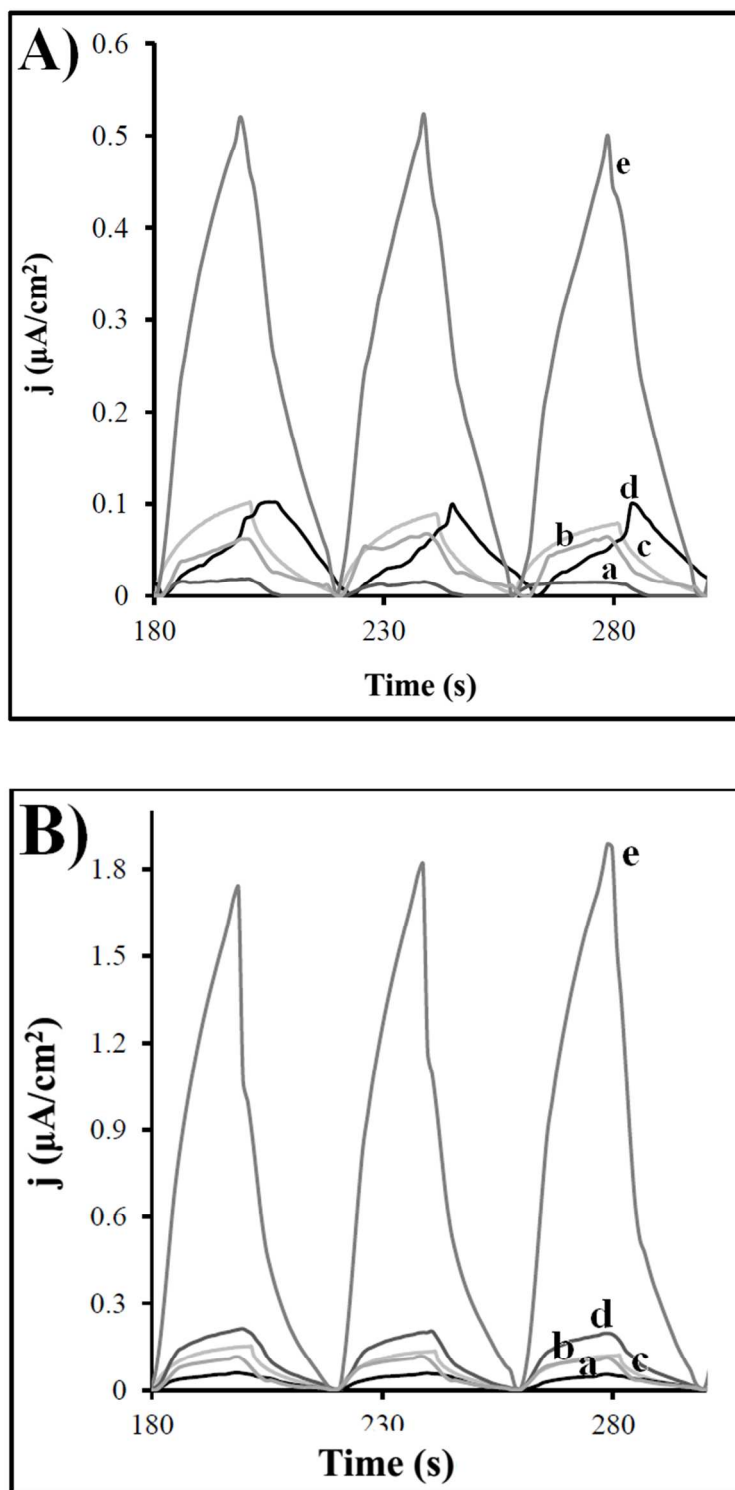
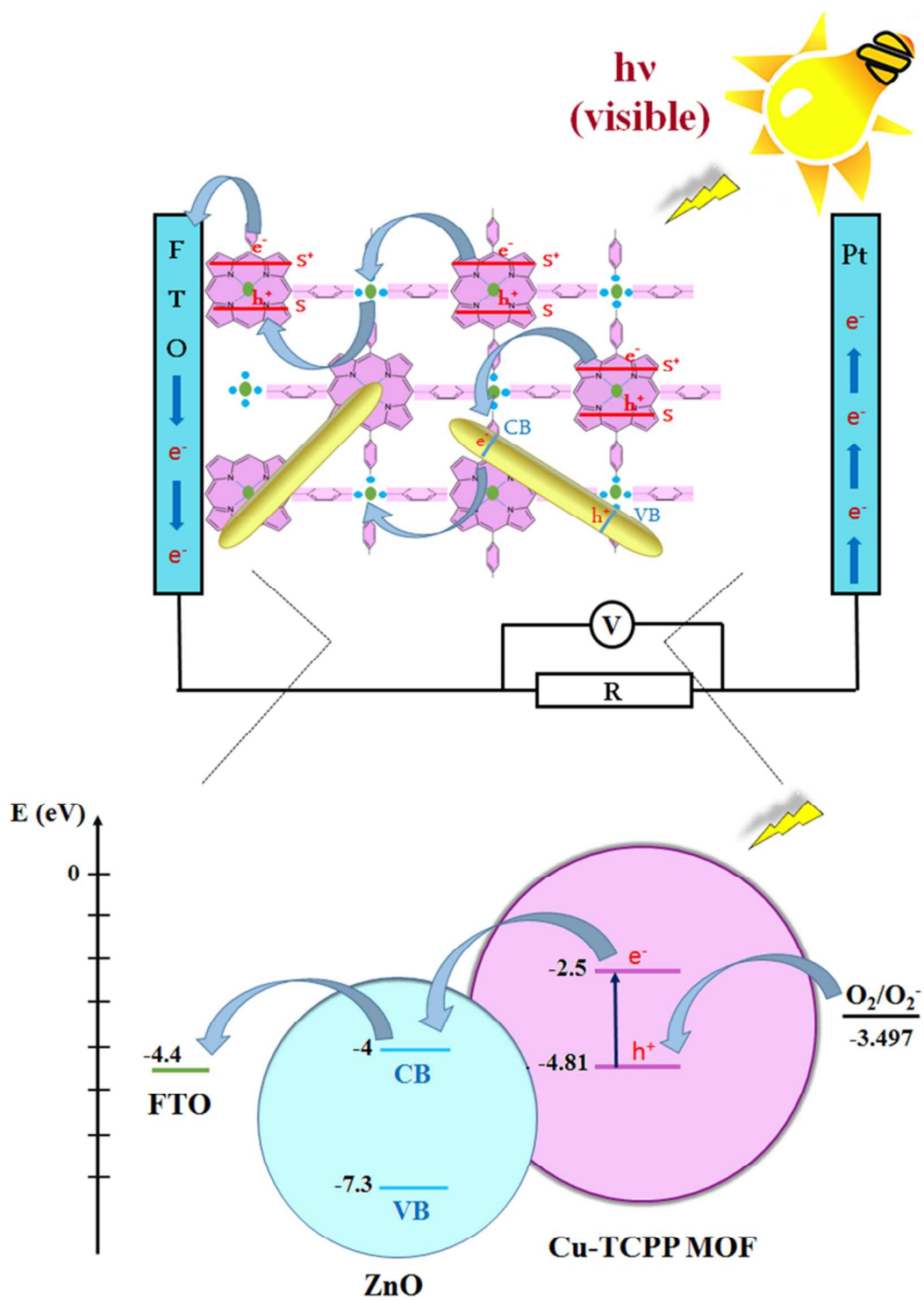
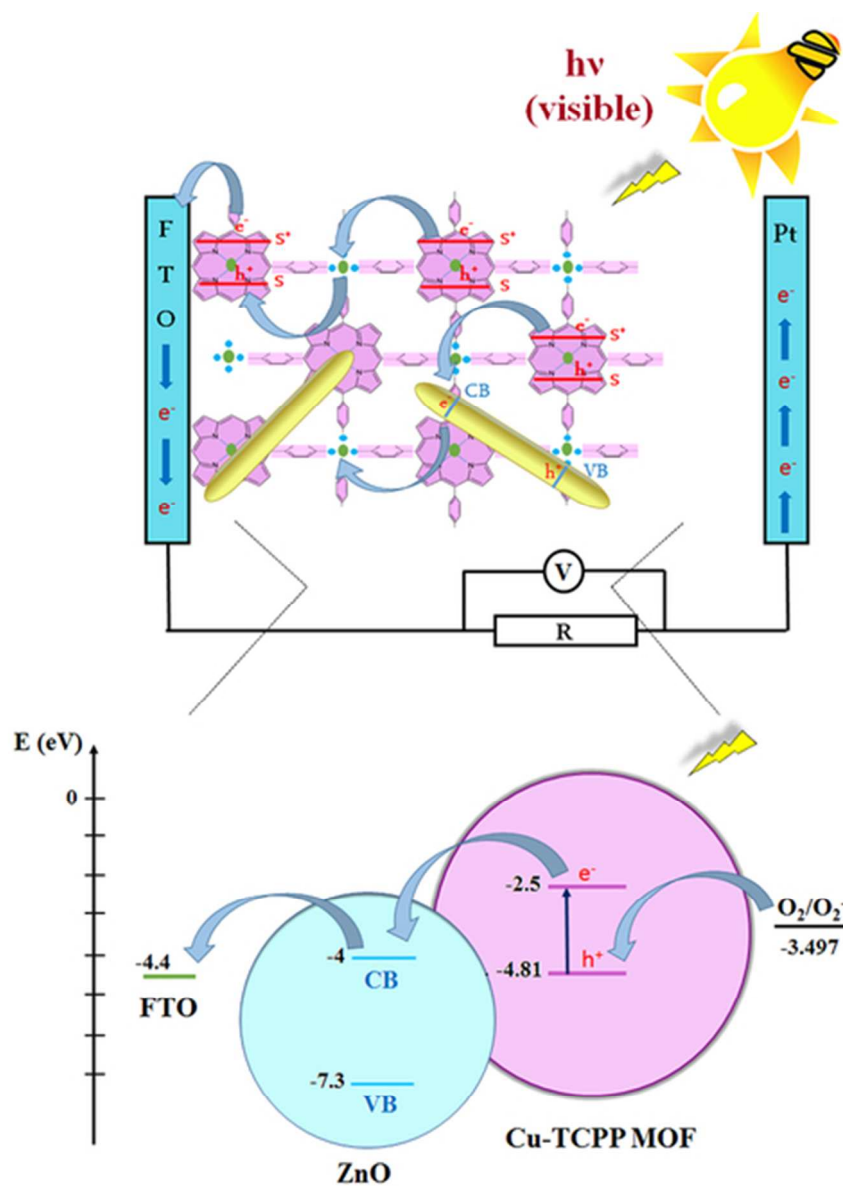


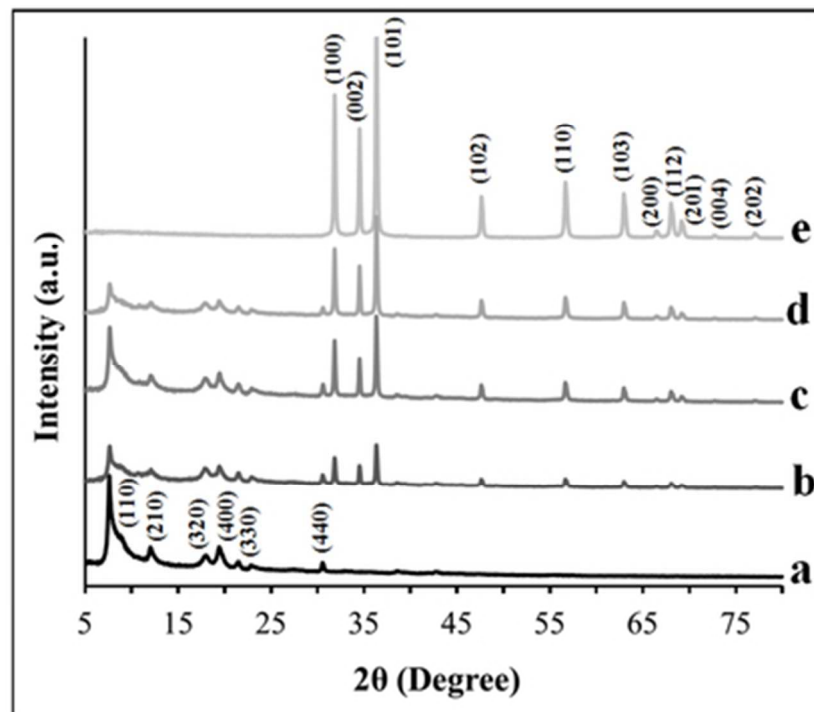
Fig. 8



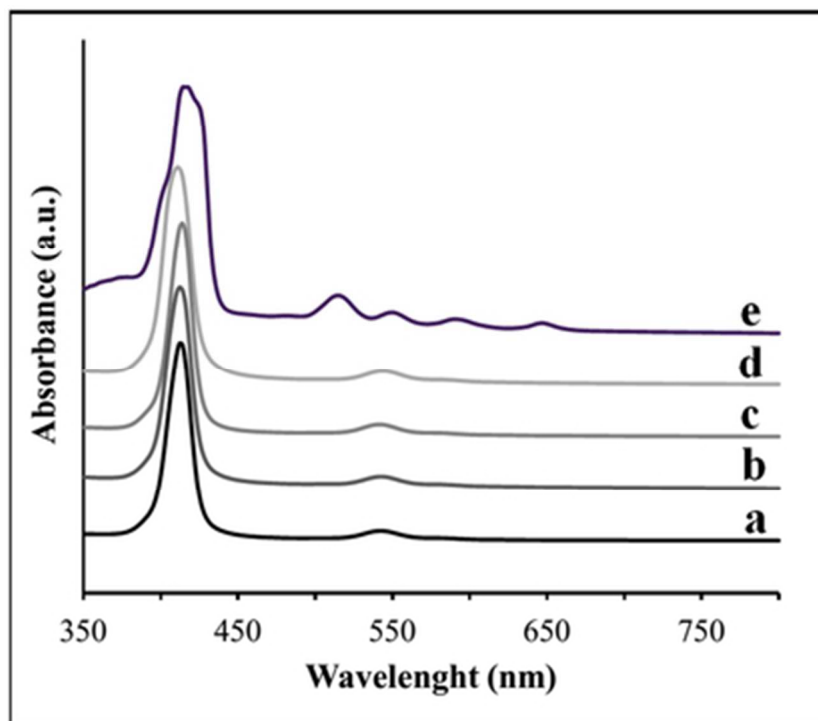
Scheme 1



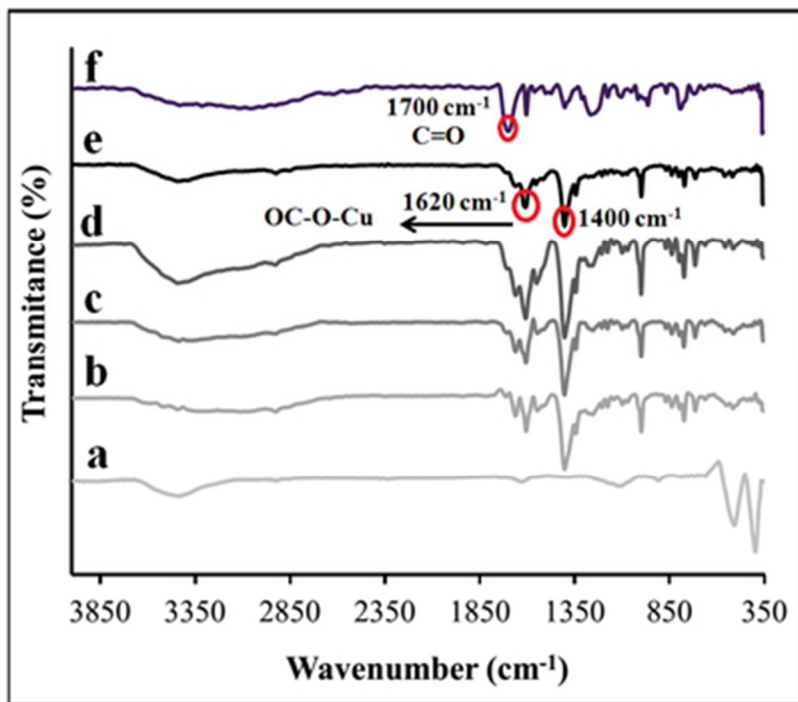
Schematic representation of the Cu-TCPP MOF/ZnO (15%) nanocomposite on an FTO substrate in the photoelectrochemical cell and the mechanism of the photocurrent generation. (the chemical potentials were calculated by cyclic voltammetry measurement.)
47x55mm (300 x 300 DPI)



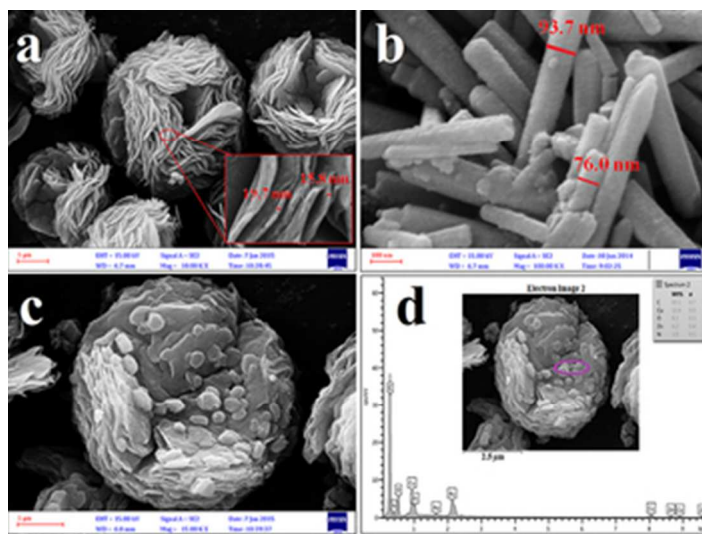
34x30mm (300 x 300 DPI)



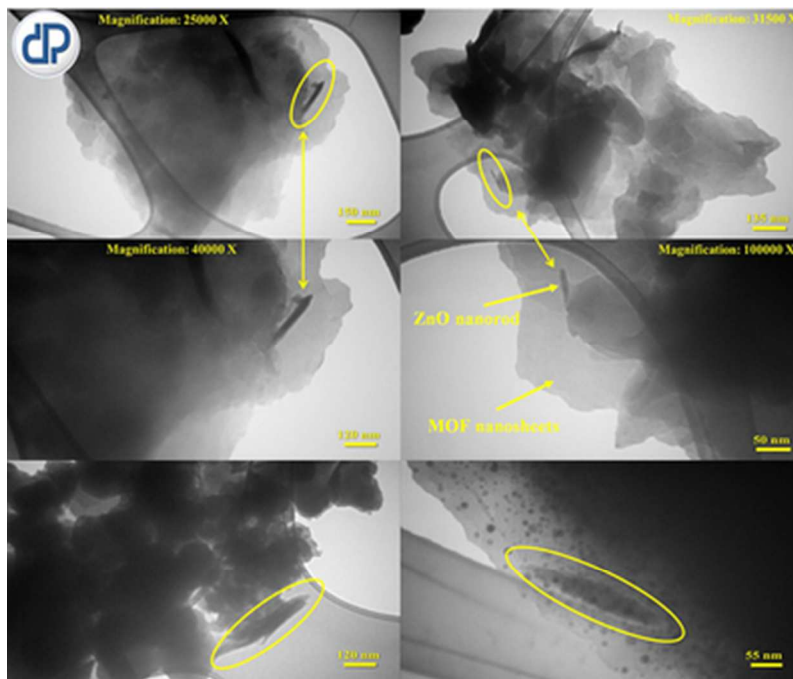
35x30mm (300 x 300 DPI)



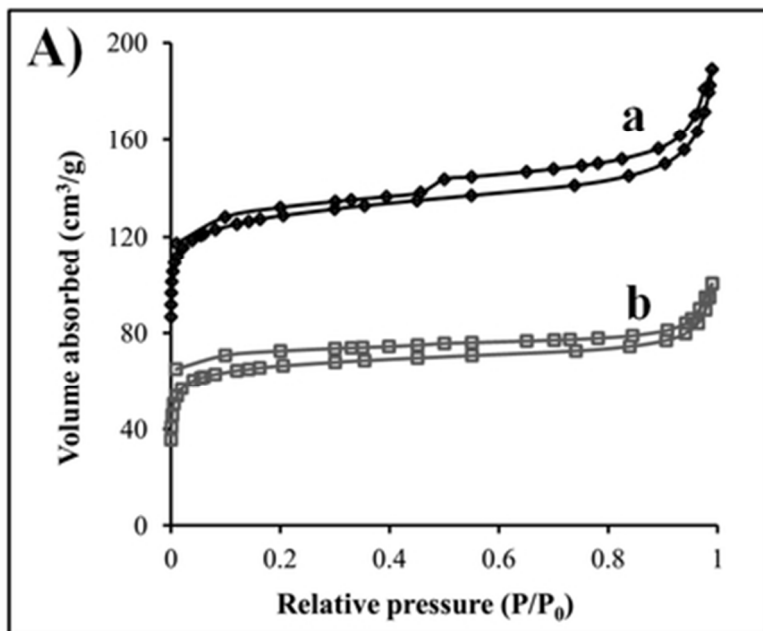
34x29mm (300 x 300 DPI)



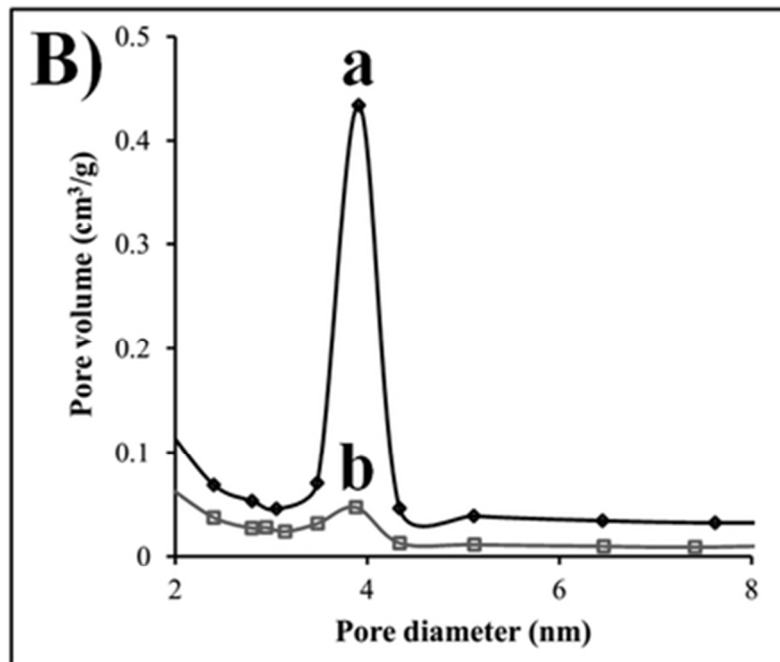
29x22mm (300 x 300 DPI)



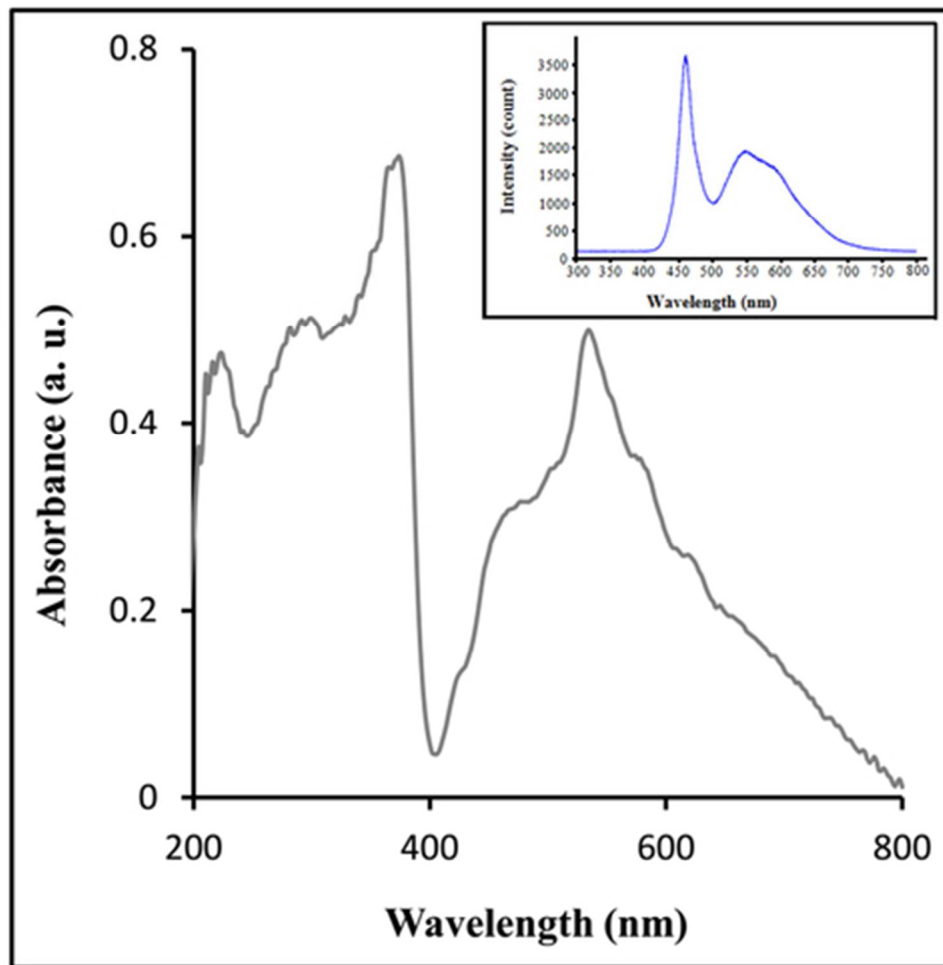
33x28mm (300 x 300 DPI)



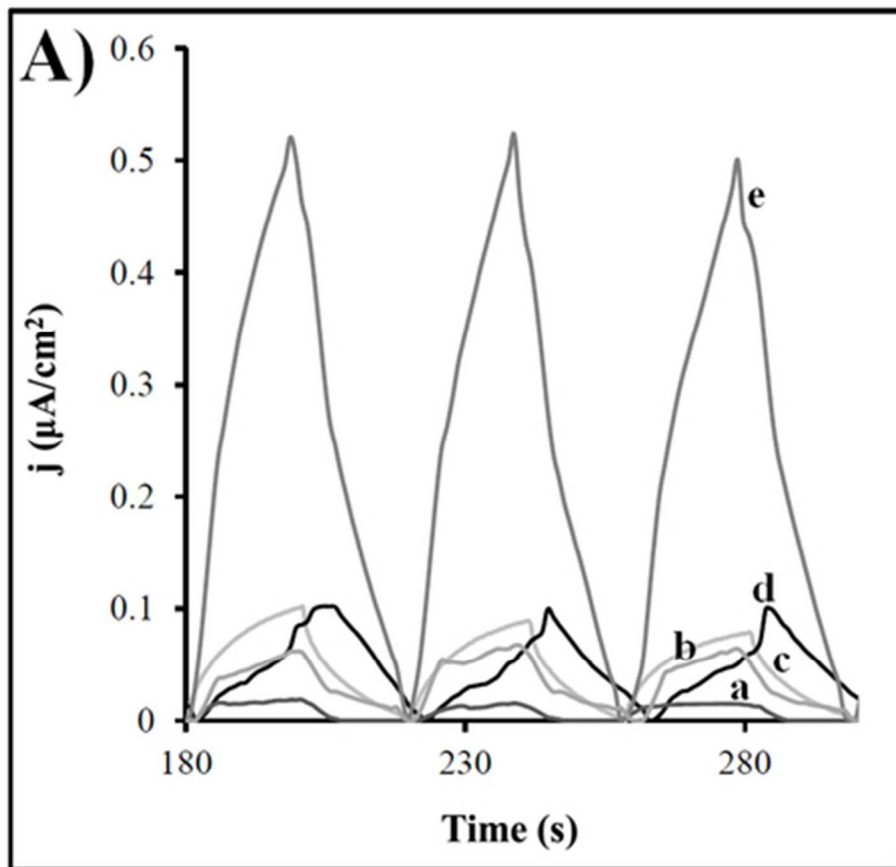
32x27mm (300 x 300 DPI)



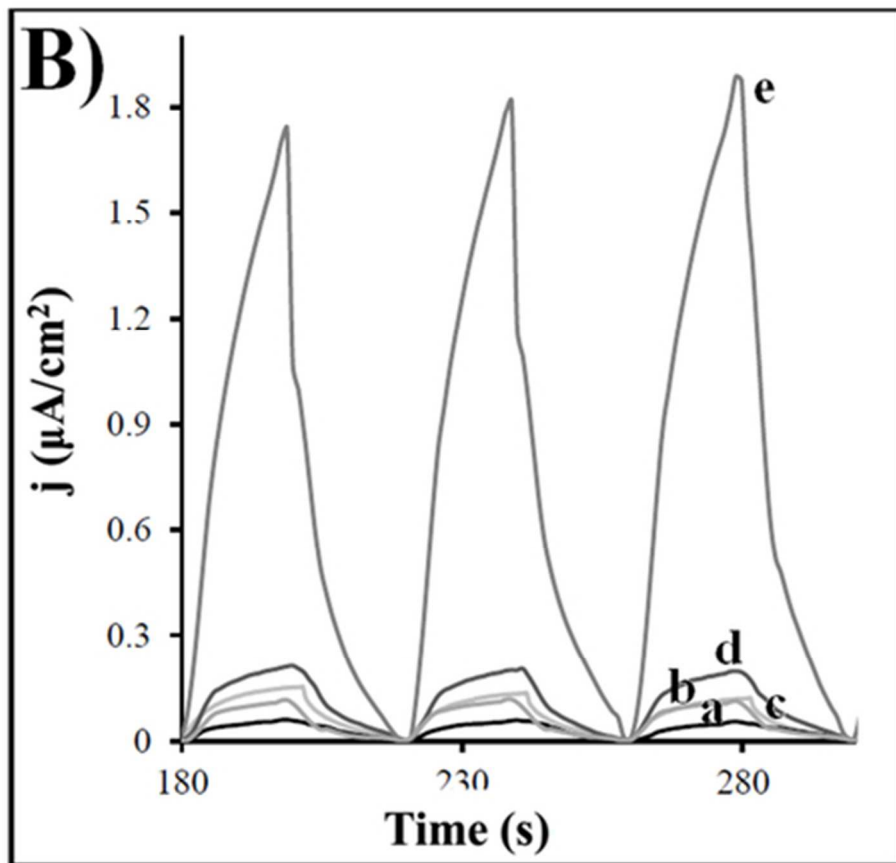
33x28mm (300 x 300 DPI)



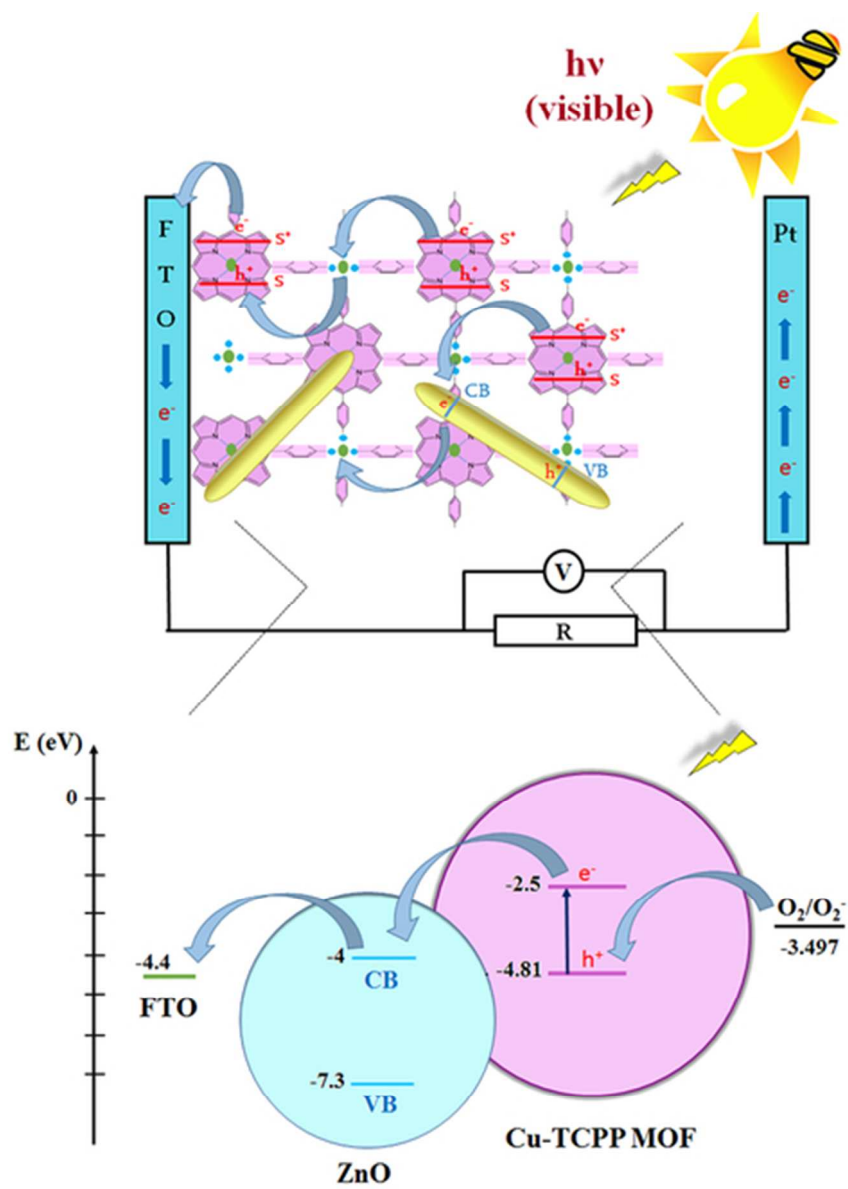
40x41mm (300 x 300 DPI)



38x36mm (300 x 300 DPI)



38x36mm (300 x 300 DPI)



47x55mm (300 x 300 DPI)